Eur. Phys. J. B **25**, 203–208 (2002)
DOI: 10.1140/epjb/e20020022

THE EUROPEAN PHYSICAL JOURNAL B
EDP Sciences

Electronic structure and metal-insulator transition in $SrTi_{1-x}Ru_xO_3$

M. Abbate[1,a], J.A. Guevara[2], S.L. Cuffini[2], Y.P. Mascarenhas[2], and E. Morikawa[3]

[1] Departamento de Física, Universidade Federal de Paraná, Caixa Postal 19091, 81531-990 Curitiba PR, Brazil
[2] Instituto de Física de São Carlos, Universidade de São Paulo, Av. Dr. C. Botelho 1465,13560-250 São Carlos SP, Brazil
[3] Center for Advanced Microstructures and Devices, Louisiana State University, 6980 Jefferson Highway, Baton Rouge, LA 70806, USA

Received 10 September 2001

Abstract. We studied the changes in the electronic structure of $SrTi_{1-x}Ru_xO_3$ across the metal-insulator transition. The parent compound, $SrTiO_3$, is a well known diamagnetic insulator; whereas the doped compound, $SrTi_{1-x}Ru_xO_3$, becomes a ferromagnetic metal above $x_C = 0.35$. The techniques used in the study were photoemission (PES) and O 1*s* X-ray absorption (XAS) spectroscopy. The experimental spectra were analyzed in terms of band structure and Hubbard model calculations. The PES and XAS spectra of $SrTi_{1-x}Ru_xO_3$ show the Ru 4*d* bands growing in the band gap of $SrTiO_3$. The analysis in terms of the Hubbard model indicates that the Ti 3*d* and Ru 4*d* bands are mostly decoupled. This suggests that the metal-insulator transition is a percolation transition like that of metals embedded in a rare gas matrix. Electron correlation effects are present in this system, but they do not seem to play a major role in the transition.

PACS. 79.60.Bm Clean metal, semiconductor, and insulator surfaces – 78.70.Dm X-ray absorption spectra – 71.30.+h Metal-insulator transitions and other electronic transitions

1 Introduction

Metal-insulator transitions induced by substitution are a relatively common occurrence in many early transition metal oxides [1]. These transitions are influenced by many factors including electron correlation, potential disorder, electron-phonon interactions, etc. Metal-insulator transitions are usually classified according to their dominant driving force: Mott-Hubbard transitions are related to electron correlation [2,3], whereas Anderson transitions are related to potential disorder [4]. In general, however, both electron correlation and potential disorder, as well as other effects, are simultaneously present in a given system. The combination of these effects produce materials which present a rich variety of phenomena and attracts considerable attention.

Typical examples of metal-insulator transitions induced by substitution in early transition metal oxides occurs in $La_{1-x}Sr_xTiO_3$ [5] and $Y_{1-x}Ca_xVO_3$ [6] (the substitution in these materials occurs at the perovskite *A*-site giving a compound of the general formula $A_{1-x}A'_xBO_3$). It is generally accepted that the dominant interaction in these materials is electron correlation within the *d*-band. These electron correlation effects are characterized by the ratio of the on-site repulsion U to the corresponding bandwidth W. A phase diagram for diverse Ti and V oxides as a function of the *d*-band filling and the relative interaction strength U/W can be found in references [7,8]. It is worth noting, however, that important disorder effects were found in the electronic structure of the related $SrTiO_{3-\delta}$ compound [9].

We study here the changes in the electronic structure of the $SrTi_{1-x}Ru_xO_3$ compound induced by Ru substitution (the substitution, in this case, occurs at the perovskite *B*-site giving a material with a $AB_{1-x}B'_xO_3$ formula). The techniques used in this study were photoemission (PES) and O 1*s* X-ray absorption (XAS) spectroscopy. The spectra of the doped $SrTi_{1-x}Ru_xO_3$ show the Ru 4*d* bands growing in the band gap of the parent $SrTiO_3$. The analysis in terms of a Hubbard model indicates that the Ti 3*d* and Ru 4*d* bands are mostly decoupled. This suggests that the metal-insulator transition is a percolation transition like that of metals embedded in a rare gas matrix [10]. Electron correlation effects are also present in this system, but unlike in the usually studied $A_{1-x}A'_xBO_3$ compounds, they do not seem to play a major role in the transition.

The physical properties of the $SrTiO_3$ and $SrRuO_3$ reference compounds are completely different. For instance, $SrTiO_3$ is a diamagnetic insulator with a cubic structure, whereas $SrRuO_3$ is a ferromagnetic metal ($T_C \simeq 150$ K) with an orthorhombic structure. Despite these differences

[a] e-mail: miguel@fisica.ufpr.br

in their physical properties, these compounds do form a continuous solid solution of the form $SrTi_{1-x}Ru_xO_3$ [11]. The electrical, magnetic and structural properties of the $SrTi_{1-x}Ru_xO_3$ series change dramatically with the Ru concentration [11–13]. In particular, the $SrTi_{1-x}Ru_xO_3$ system presents an insulator to metal transition for a Ru concentration above $x_C \simeq 0.35$. At this critical concentration, the material becomes also ferromagnetic and presents a cubic to orthorhombic transition.

2 Experimental details

The $SrTi_{1-x}Ru_xO_3$ samples were prepared using the solid state reaction method [14]. The resulting powders were pressed into pellets and sintered in air at 1100 °C for 24 hours. The powder X-ray diffraction (XRD) analysis confirmed that the samples were all single phase [14]. The absence of superstructure in the XRD indicated that the Ti and Ru ions were randomly distributed. This confirms that the samples form a solid solution and are not a mixture of two compounds. More details on the sample preparation and characterization will be published elsewhere.

The experiment was carried out at the plane-grating monochromator (PGM) beamline in CAMD [15]. The base pressure in the experimental chamber was in the low 10^{-9} mbar range. The photoemission spectra were measured using an hemispherical electrostatic analyzer. The photon energy was 40 eV and the Fermi level was calibrated using a Cu foil cleaned by sputtering. The overall energy resolution of PES estimated from the Cu Fermi edge was approximately 300 meV. The O 1*s* X-ray absorption spectra were measured using the total electron yield method. The energy scale in the XAS spectra was calibrated using the known peak positions in $SrTiO_3$. The energy resolution at the O 1*s* X-ray absorption edge was approximately 0.5 eV. The samples were scraped *in situ* with a diamond file to remove surface contamination.

3 Results and discussion

3.1 Photoemission and X-ray absorption

Figure 1 shows the photoemission (PES) spectra of $SrTi_{1-x}Ru_xO_3$ as a function of the Ru concentration x. In a first approximation the spectra reflect the occupied electronic states in the valence band. The spectrum of $SrTiO_3$ presents two broad and overlapping bumps around −5 and −7 eV which are attributed to the O 2*p* bands. This spectrum is in good agreement with both previous photoemission results and LDA band structure calculations [5,16]. The spectra of the doped compound $SrTi_{1-x}Ru_xO_3$ present changes in the O 2*p* band region and a growing shoulder around −9 eV. These changes resemble closely the dominant features in the photoemission spectrum of the end member of the series $SrRuO_3$ [17,18]. Moreover, the spectra of the doped compound present additional spectral weight close to the Fermi level which is attributed to the Ru 4*d* bands. The absence of spurious intensity around −10 eV, which is usually attributed to surface contamination, confirms the surface cleanness [19].

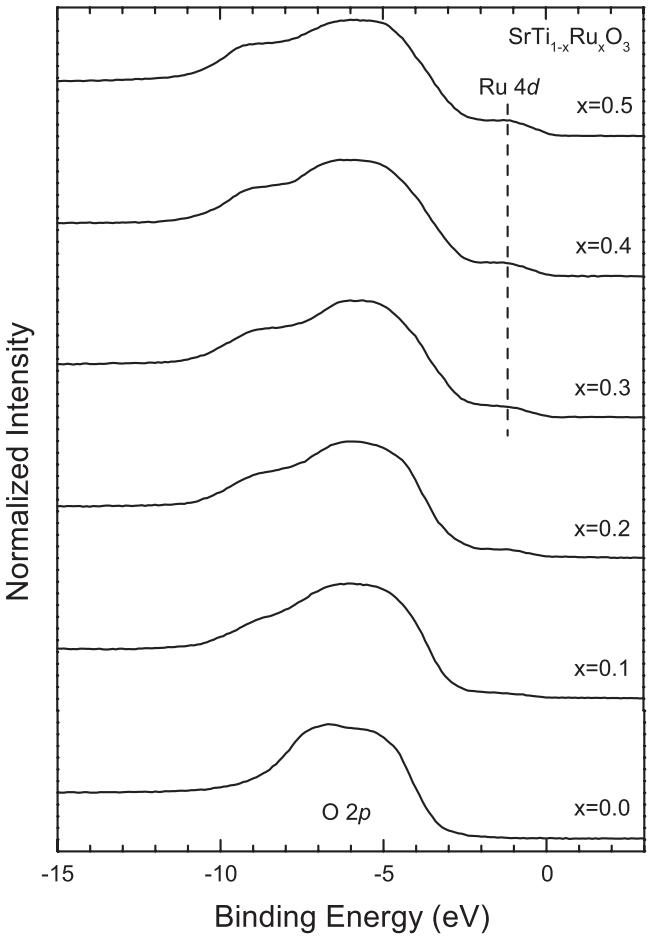

Fig. 1. Photoemission spectra of $SrTi_{1-x}Ru_xO_3$ as a function of the Ru concentration x.

Figure 2 shows the O 1*s* X-ray absorption (XAS) spectra of $SrTi_{1-x}Ru_xO_3$ as a function of the Ru concentration x. In a first approximation the spectra map the unoccupied electronic states in the conduction band. The spectrum of $SrTiO_3$ presents the Ti 3*d* band region at threshold, the Sr 4*d* region around 536–539 eV, and the Ti 4*sp* region around 542–546 eV. This spectrum is in excellent agreement with both previous X-ray absorption results and LDA band structure calculations [5,16]. The spectra of the doped compound $SrTi_{1-x}Ru_xO_3$ present smooth changes throughout as the Ti derived regions evolve into Ru derived features. Again, these changes resemble very closely the main features in the X-ray absorption spectrum of the end member of the series $SrRuO_3$ [17, 18]. The most relevant change is the emerging peak below the edge of the parent compound around 539.5 eV which is attributed to the Ru 4*d* bands.

Figure 3 shows the PES and O 1*s* XAS spectra of $SrTi_{1-x}Ru_xO_3$ close to the Fermi level as a function of the Ru concentration x. These low energy states are particularly relevant because they can be directly related

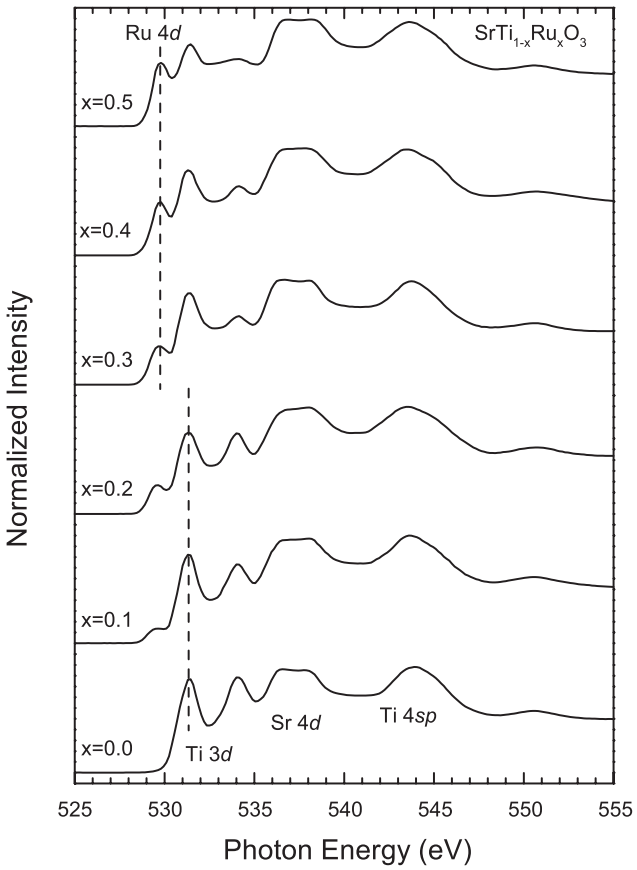

Fig. 2. O 1*s* X-ray absorption spectra of $SrTi_{1-x}Ru_xO_3$ as a function of the Ru concentration x.

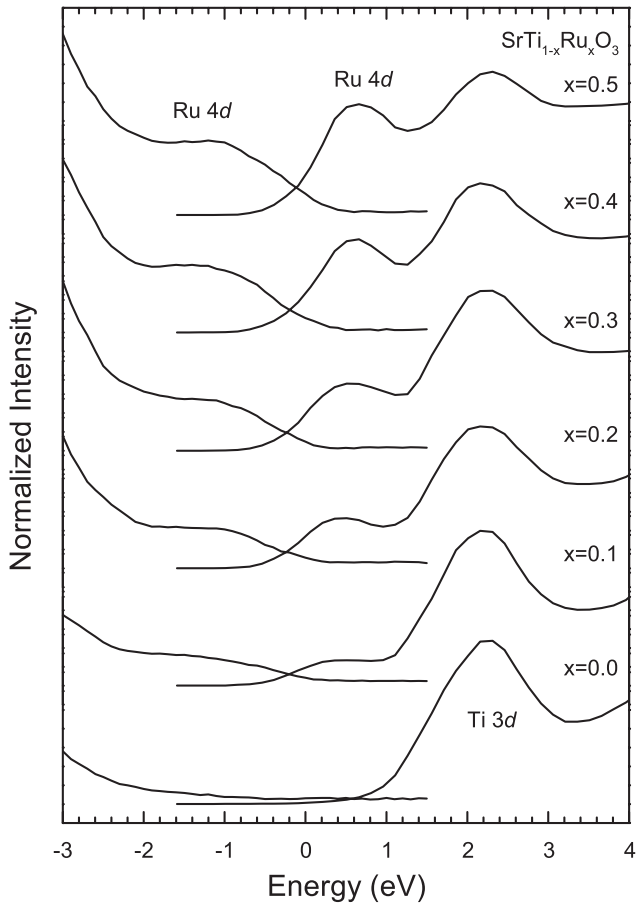

Fig. 3. Photoemission and O 1*s* X-ray absorption spectra of $SrTi_{1-x}Ru_xO_3$ as a function of the Ru concentration x.

to the physical properties of the compounds. The PES spectra were normalized to the intensity at −15 eV and the O 1*s* XAS spectra to the intensity at 555 eV; this is justified because the intensity at these particular points does not depend on the Ru concentration. The Fermi level in the O 1*s* XAS spectra was determined by the position of the absorption edge in metallic $SrTi_{0.5}Ru_{0.5}O_3$, this procedure is justified *a posteriori* because the resulting band gap for $SrTiO_3$ is in reasonable agreement with experiment.

The PES spectrum of $SrTiO_3$ presents the onset of the O 2*p* band below −2.2 eV, which corresponds to the top of the valence band. The O 1*s* XAS spectrum of $SrTiO_3$ presents the onset of the Ti 3*d* band above 1.0 eV, which corresponds to the bottom of the conduction band. The unoccupied Ti 3*d* states are split by crystal field effects into the t_{2g} and e_g sub-bands at 2.3 and 4.5 eV (not shown), respectively. The crystal field splitting $10Dq$ between the t_{2g} and e_g sub-bands, 2.2 eV, is in good agreement with previous results [16]. The combination of the band edges in the PES and O 1*s* XAS spectra gives a band gap of approximately 3.2 eV for $SrTiO_3$; this value is in good agreement with the experimental band gap of 3.2 eV derived from optical measurements [20].

The PES and O 1*s* XAS spectra of the doped compound $SrTi_{1-x}Ru_xO_3$ show an increasing spectral weight filling the band gap of $SrTiO_3$. This spectral weight increase is attributed to the gradual development of the Ru 4*d* derived band. The evolution of the Ru 4*d* band does not involve a shift of the Fermi level and is consistent with the so called *in gap* states scenario. A (rigid band) shift of the Fermi level to the bottom of the $SrTiO_3$ conduction band and the ensuing population of Ti 3*d* states is not observed. The overall shape, band width and peak position of the Ru 4*d* derived bands do not change with the Ru concentration. On the other hand, the total intensity of the Ru 4*d* derived bands grows linearly with the Ru concentration x. In fact, the spectral weight of the doped compound resembles a linear combination of the spectra of the two end members. It is worth noting that the DOS at the Fermi level seems to be finite even for the insulating samples with $x \leq 0.35$, see below.

3.2 Comparison to LDA calculations

Band structure calculations based on the LDA approximation provides a useful framework to analyze the PES and O 1*s* XAS spectra. The assignments in the PES and O 1*s* XAS spectra made above are partially justified by the results of previous LDA calculations [16,17]. The bottom of Figure 4 presents the band structure calculation of $SrTiO_3$ from reference [16] shifted to match the

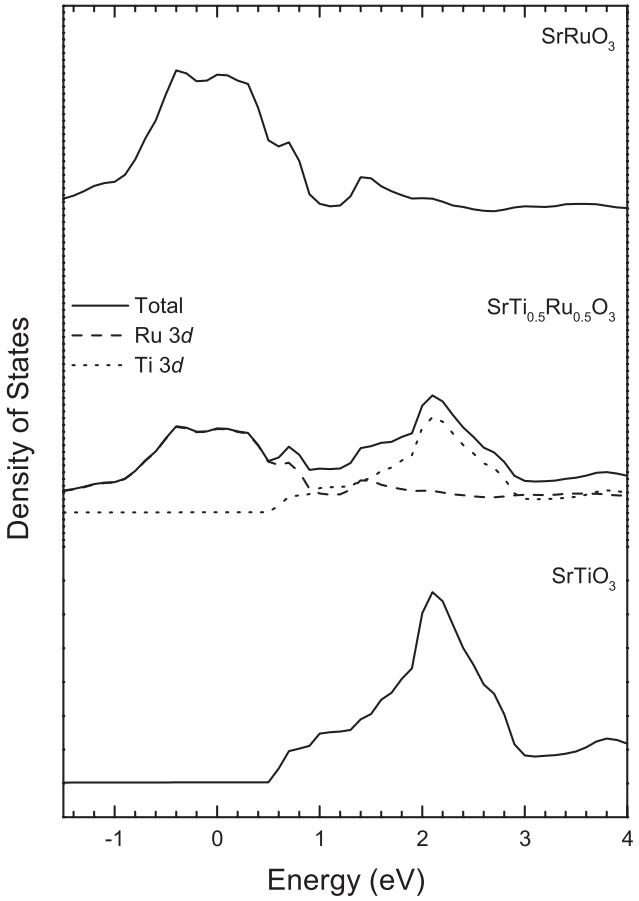

Fig. 4. Band structure calculation for (a) $SrTiO_3$ (Ref. [16]), (b) $SrTi_{0.5}Ru_{0.5}O_3$ ($SrTiO_3$ + $SrRuO_3$), and (c) $SrRuO_3$ (Ref. [18]).

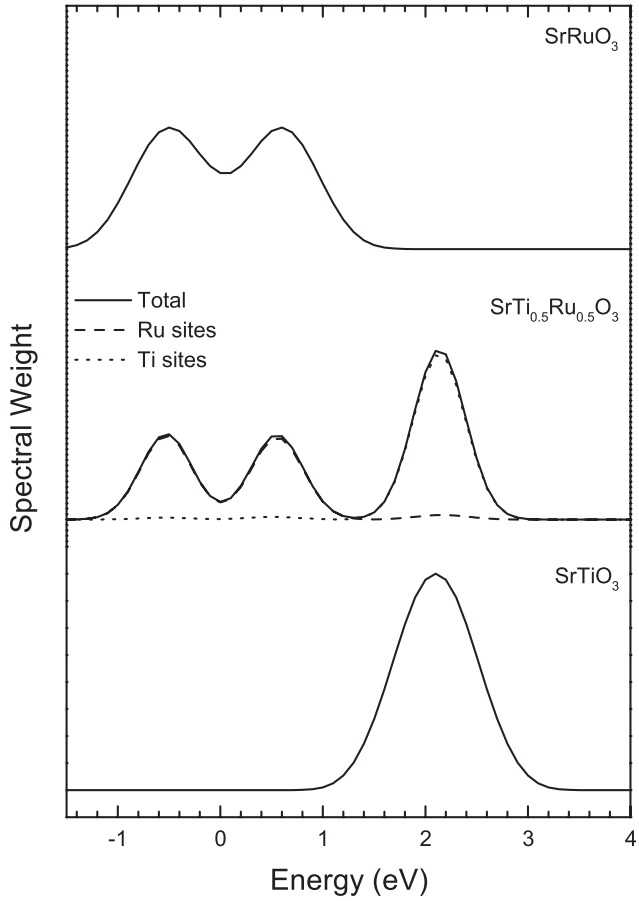

Fig. 5. Calculated spectral function of the Hubbard model for (a) $SrTiO_3$, (b) $SrTi_{0.5}Ru_{0.5}O_3$, and (c) $SrRuO_3$.

position of the Ti 3*d* band (the calculation underestimates the value of the band gap and places the Fermi level at the top of the valence band). The top of Figure 4 presents the band structure calculation of $SrRuO_3$ from reference [18] with the Ru 4*d* bands located at the Fermi level.

The middle of Figure 4 shows the DOS for $SrTi_{0.5}Ru_{0.5}O_3$ obtained as a 1:1 linear combination of the results for $SrTiO_3$ and $SrRuO_3$. This method reproduces reasonably well the main features observed in the PES and O 1*s* XAS spectra of $SrTi_{1-x}Ru_xO_3$. The agreement of the linear combination with the experimental spectra suggests that the Ti 3*d* and Ru 4*d* bands are mostly decoupled, which means that the Ti 3*d* states are not covalently mixed with the Ru 4*d* states and *vice versa*, see below. This is reasonable because the energy separation between the bands ΔE (1.8 eV) is larger than the corresponding bandwidth W (1.2 eV). An additional justification for the linear combination used here is provided by the results of the Hubbard model calculation below.

3.3 Hubbard model calculation

To understand the decoupling of the Ti 3*d* and Ru 4*d* bands in $SrTi_{1-x}Ru_xO_3$ we consider a simple Hubbard model with one orbital per site:

$$H = \sum_{i\sigma} \epsilon_i \, n_{i\sigma} - \sum_{\langle ij\rangle\sigma} t_{ij} \, (c^{\dagger}_{i\sigma} \, c_{j\sigma} + \text{h.c.}) + \sum_{i} U_i \, n_{i\uparrow} \, n_{i\downarrow}$$

where $c^{\dagger}_{i\sigma}$ ($c_{i\sigma}$) creates (destroys) an electron at site i with spin σ and $n_{i\sigma} = c^{\dagger}_{i\sigma} \, c_{i\sigma}$. The parameters of the model are the on-site electron energy ϵ_i , the nearest-neighbor electron transfer t_{ij}, and the on-site electron-electron repulsion U_i. The model is solved using the configuration interaction method in a $2 \times 2 \times 2$ cubic cluster with periodic boundary conditions. The index i denotes each of the sites in the cluster lattice and the symbol $\langle ij\rangle$ denotes a summation over nearest-neighbors. The Ru sites contribute with one electron, the Ti sites contributes with no electron, and the ground state is chosen to be ferromagnetic. The results of the calculation were broadened with a 0.5 eV Gaussian to take into account the experimental resolution. The value of the parameters used here were obtained by matching the features in the experimental spectra.

The bottom of Figure 5 shows the results of the model calculation for $SrTiO_3$ obtained with all the sites in the cluster occupied by Ti ions. The energy ϵ_{Ti}, 2.1 eV, was deduced from the peak position in the O 1*s* XAS spectrum

and the transfer t_{Ti-Ti}, 0.12 eV, from the peak width [21]. As the ground state in this case corresponds to an empty band there is no many-body effects and the repulsion U_{Ti} remains undetermined. The results of the model calculation for $SrTiO_3$ are in reasonable agreement with both the experimental spectra and the LDA calculation.

The top of Figure 5 shows the results of the model calculation for $SrRuO_3$ obtained with all the sites in the cluster occupied by Ru ions. The energy ϵ_{Ru}, -0.5 eV, and transfer t_{Ru-Ru}, 0.10 eV, were deduced from the peak position and width in both the experimental spectra and the LDA calculation. The value of the repulsion U_{Ru} used here, 1.1 eV, represents an upper limit as larger values would result in a correlation gap within this model. As the ground state, in this case, corresponds to a completely filled majority spin band there is no many-body satellites. The results of the model calculation for $SrRuO_3$ resembles reasonably well both the experimental spectra and the LDA calculation.

The middle of Figure 5 shows the results of the model calculation for $SrTi_{0.5}Ru_{0.5}O_3$ obtained with Ti and Ru ions occupying alternate sites. The values of the energies ϵ_i and repulsion U_i for the Ti and Ru ions were taken from the simulation for $SrTiO_3$ and $SrRuO_3$ above, and the value of the transfer t_{Ti-Ru} was obtained by interpolation of the transfer t_{Ti-Ti} and t_{Ru-Ru} values. Dispersion and double-occupancy are strongly inhibited because the energy difference $\epsilon_{Ti} - \epsilon_{Ru}$ is much larger than the transfer t_{Ti-Ru}. The restricted dispersion produces narrower bands and the reduced double-occupancy results in negligible many-body satellites. More important, the relatively large energy difference $\epsilon_{Ti} - \epsilon_{Ru}$ with respect to t_{Ti-Ru} effectively decouples the Ti $3d$ and Ru $4d$ bands. This can be confirmed by the decomposition of the total spectral weight into the Ti and Ru partial weight in the middle of Figure 5. This provides a justification for the simulation of the $SrTi_{0.5}Ru_{0.5}O_3$ band in term of a 1:1 linear combination of $SrTiO_3$ and $SrRuO_3$ made above. It is worth noting that the spectral weight at the Fermi level corresponds almost entirely to Ru $4d$ states. The results of the model calculation for $SrTi_{0.5}Ru_{0.5}O_3$ reproduces the main features in both the experimental spectra and the LDA calculation.

One might question the validity of the conclusions based on this simple Hubbard model calculations from various viewpoints. First, the true ground state of this model is antiferromagnetic because this favors charge fluctuations and lowers the kinetic energy. The ground state in our case was constrained to be ferromagnetic to take into account the observed magnetic ordering of the compound. Secondly, the Ru ions are randomly distributed in the crystal lattice whereas the calculation was performed using an alternate distribution. The effect of disorder can be ruled out because calculations with Ru ions located at random positions gave similar results. Thirdly, the results might not be representative because of the relatively small cluster size ($2 \times 2 \times 2$) used in the calculations. But restricted Hartree-Fock calculations on a $4 \times 4 \times 4$ cluster, with the occupancy fixed to that of the configuration interaction model, gave similar results. Finally, a model with only one orbital per site does not take into account the six-fold degeneracy of the Ru t_{2g} sub-band. But the effect of the degeneracy is not so critical in this case because $SrRuO_3$ is close to be an itinerant band ferromagnet. A larger size, disordered and degenerate model calculation would be certainly more realistic, but it is beyond the scope of the present work.

3.4 Metal-insulator transition

The electronic structure and metal-insulator transition of early transition metal oxides are influenced by various factors. These factors include, for example, electron correlation, potential disorder, and electron-phonon interactions, among others. It is usually accepted that the dominant interaction in these materials is electron correlation within the transition metal d-band. The relative importance of these effects is given by the ratio U/W of the on-site repulsion U to the corresponding bandwidth W. In this case, a metal-insulator transition is expected whenever the ratio U/W is larger than a certain critical value. This is the case for most $A_{1-x}A'_xBO_3$ systems like $La_{1-x}Sr_xTiO_3$, but it is not generally true for a $AB_{1-x}B'_xO_3$ system like $SrTi_{1-x}Ru_xO_3$.

In $SrTi_{1-x}Ru_xO_3$, the energy separation between the Ti $3d$ and Ru $4d$ bands ΔE is larger than the corresponding bandwidths W (in terms of the Hubbard model parameters, the on-site energy difference $\epsilon_{Ti} - \epsilon_{Ru}$ is larger than the transfer integral t_{Ti-Ru}). This effect decouples the Ti $3d$ and Ru $4d$ bands preventing charge fluctuations from the Ru $4d$ states at the Fermi level to Ti $3d$ states. In view of this, we propose that the metal-insulator transition in $SrTi_{1-x}Ru_xO_3$ is a percolation transition like that of metals embedded in a rare gas matrix [10]. This proposition makes sense because the critical Ru concentration, $x_C \simeq 0.35$, is similar to the onset of percolation on a simple cubic lattice, $x_C \simeq 0.31$ [22]. Electron correlation effects are certainly present in this system and affect the details of the spectral weight distribution close to the Fermi level. The absence of changes in the shape of the spectra across x_C suggests, however, that these effects do not play a major role in the transition.

This would represent a different mechanism for a metal-insulator transition in $AB_{1-x}B'_xO_3$ early transition metal oxides. This type of transition would be characterized by the ratio $\Delta E/W$ of the band separation ΔE to the corresponding bandwidth W. In fact, this transition could be regarded as a special case of the metal-insulator transition driven by potential disorder (Anderson localization). Below the percolation threshold, a metal-insulator transition would be expected for a $\Delta E/W$ ratio larger than a certain critical value. On the other hand, above the percolation threshold, the system would be metallic even for relatively large $\Delta E/W$ ratios. These arguments would apply only in the absence of other localization effects, like electron correlation and electron-phonon interactions. It is worth noting, that the ratio $\Delta E/W$ was already invoked

to rationalize the differences in the metal-insulator transition of $LaNi_{1-x}M_xO_3$ compounds (M = Mn, Fe, Co) [23].

The experimental spectra show a finite DOS at the Fermi level even for the insulating samples below the critical concentration $x_C \simeq 0.35$. This spectral weight, however, corresponds to localized Ru 4*d* states and not to delocalized states, because the energy separation between the bands ΔE prevents charge fluctuations from Ru 4*d* states at the Fermi level to Ti 3*d* states. The same kind of behavior, with a finite DOS at the Fermi level, was observed in the valence band spectra of insulating Fe-Al_2O_3 [24]. In this granular system, metallic Fe precipitates are embedded, below the percolation threshold, in an insulating Al_2O_3 matrix. In fact, the $SrTi_{1-x}Ru_xO_3$ solid solution studied here could be regarded as the dilution limit of a $SrRuO_3$-$SrTiO_3$ granular alloy.

The metal-insulator transition around $x_C \simeq 0.35$ in $SrTi_{1-x}Ru_xO_3$ is accompanied by a crystallographic transition. In the insulating phase below x_C the compound is cubic, whereas in the metallic phase above x_C it becomes orthorhombic. The cubic structure has straight M-O-M chains which gives rise to a larger bandwidth and favors metallic behavior. On the other hand, the orthorhombic structure has distorted M-O-M chains which results in a reduced bandwidth and is prejudicial to the metallic state. This means that the crystal structure would favor the metallic state below x_C which is at variance with the observed behavior. This shows clearly that the metal-insulator transition in this compound is not driven by the crystallographic transition. This unrelated crystallographic transition is caused by the differences in the ionic radii of the Ti and Ru ions [14].

4 Summary and conclusions

In summary, we studied the changes in the electronic structure of $SrTi_{1-x}Ru_xO_3$ across the metal-insulator transition at $x_C \simeq 0.35$. The techniques used in this study were photoemission (PES) and O 1*s* X-ray absorption spectroscopy (XAS). The experimental spectra were analyzed in terms of band structure and Hubbard model calculations. The spectra of the doped compound, $SrTi_{1-x}Ru_xO_3$, show the Ru 4*d* bands growing in the band gap of $SrTiO_3$. The analysis based on the Hubbard model indicates that the Ti 3*d* and Ru 4*d* bands are mostly decoupled. The energy separation between the bands prevents charge fluctuations from the Ru 4*d* states at the Fermi level to Ti 3*d* states. This suggests that the metal-insulator transition is a percolation transition like that of metals embedded in a rare gas matrix. Electron correlation effects are present in this system, but they do not seem to play a major role in the transition.

This work was partially supported by CNPq, PRONEX, and NSF. The operation of CAMD is supported by the State of Louisiana.

References

1. M. Imada, A. Fujimori, Y. Tokura, Rev. Mod. Phys. **70**, 1039 (1998).
2. N.F. Mott, Proc. Phys. Soc. London A **62**, 416 (1949).
3. J. Hubbard, Proc. R. Soc. London A **277**, 237 (1964); **281**, 401 (1964).
4. P.W. Anderson, Phys. Rev. **109**, 1492 (1958).
5. A. Fujimori, I. Hase, M. Nakamura, H. Namatame, Y. Fujishima, Y. Tokura, M. Abbate, F.M.F. de Groot, M.T. Czyzyk, J.C. Fuggle, O. Strebel, F. Lopez, M. Domke, G. Kaindl, Phys. Rev. B **46**, 9841 (1992).
6. H.F. Pen, M. Abbate, A. Fujimori, Y. Tokura, H. Eisaki, S. Uchida, G.A. Sawatzky, Phys. Rev. B **59**, 7422 (1999).
7. A. Fujimori, I. Hase, Y. Tokura, M. Abbate, F.M.F. de Groot, J.C. Fuggle, H. Eisaki, S. Uchida, Physica B **186-188**, 981 (1993).
8. K. Morikawa, T. Mizokawa, A. Fujimori, Y. Taguchi, Y. Tokura, Phys. Rev. B **54**, 8446 (1996).
9. D.D. Sarma, S.R. Barman, H. Kajueter, G. Kotliar, Europhys. Lett. **36**, 307 (1996).
10. N.F. Mott, *Conduction in Non-Cristalline Materials* (Clarendon, Oxford, 1993).
11. S.L. Cuffini, V.A. Macagno, R.E. Carbonio, A. Melo, E. Trollund, J.L. Gautier, J. Solid State Chem. **105**, 161 (1993).
12. S.L. Cuffini, R.A. Carbonio, Ferroelectrics **155**, 165 (1994).
13. H.R. Oswald, S. Felder-Casagrande, A. Reller, Solid State Ionics **63-65**, 565 (1993).
14. J.A. Guevara, Ph.D. thesis, Universidade de São Paulo (1998).
15. E. Morikawa, J.D. Scott, E.D. Poliakoff, R.L. Stockbauer, V. Saile, Rev. Sci. Instrum. **63**, 1300 (1992).
16. F.M.F. de Groot, J. Faber, J.J.M. Michiels, M.T. Czyzyk, M. Abbate, J.C. Fuggle, Phys. Rev. B **48**, 2074 (1993).
17. K. Fujioka, J. Okamoto, T. Mizokawa, A. Fujimori, I. Hase, M. Abbate, H.J. Lin, C.T. Chen, Y. Takeda, M. Takano, Phys. Rev. B **56**, 6380 (1997).
18. J. Okamoto, T. Mizokawa, A. Fujimori, I. Hase, M. Nohara, H. Takagi, Y. Takeda, M. Takano, Phys. Rev. B **60**, 2281 (1999).
19. T. Saitoh, A.E. Bocquet, T. Mizokawa, H. Namatame, A. Fujimori, M. Abbate, Y. Takeda, M. Takano, Phys. Rev. B **51**, 13942 (1995).
20. M. Cardona, Phys. Rev. **140**, A651 (1965).
21. The width of the band W is given by $12t$ because each nearest-neighbor contributes $2t$ to the width and there are 6 nearest-neighbors in a cubic lattice.
22. D. Stauffer, A. Aharony, *Introduction to Percolation Theory* (Taylor and Francis, London, 1994).
23. D.D. Sarma, A. Chainani, S.R. Krishnakumar, E. Vescovo, C. Carbone, W. Eberhardt, O. Rader, Ch. Jung, Ch. Hellwig, W. Gudat, H. Srikanth, A.K. Raychaudhuri, Phys. Rev. Lett. **80**, 4004 (1998).
24. C.A.M. Pereira, M. Abbate, W.H. Schreiner, M.A.S. Boff, S.R. Teixeira, J.E. Schmidt, Solid State Commun. **116**, 457 (2000).